

1      **Impact of grids and dynamical cores in CESM2.2 on**  
2      **the meteorology and climate of the Arctic**

3      **Adam R. Herrington** <sup>1</sup>, **Marcus Lofverstrom** <sup>2</sup>, **Peter H. Lauritzen** <sup>1</sup> and  
4      **Andrew Gettelman** <sup>1</sup>

5      <sup>1</sup>National Center for Atmospheric Research, 1850 Table Mesa Drive, Boulder, Colorado, USA  
6      <sup>2</sup>Department of Geosciences, University of Arizona, 1040 E. 4th Street, Tucson, AZ USA

7      **Key Points:**

- 8      • enter point 1 here  
9      • enter point 2 here  
10     • enter point 3 here

**Abstract**

[ enter your Abstract here ]

**Plain Language Summary**

[ enter your Plain Language Summary here or delete this section]

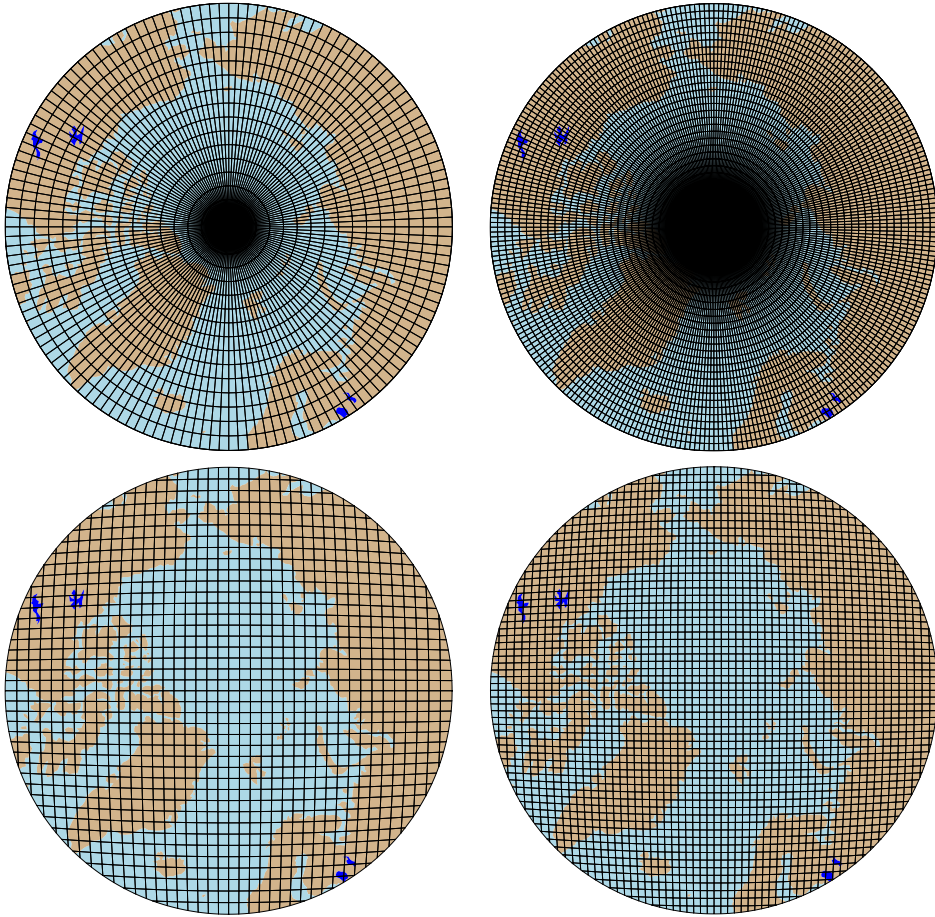
**1 Introduction**

General Circulation Models (GCMs) are powerful tools for understanding the meteorology and climate of the high-latitudes, which are among the most sensitive regions on Earth to global and environmental change. Despite their importance, the numerical treatment of polar regions is handled in vastly-different ways due to the so-called *pole-problem* (Williamson, 2007). The pole-problem refers to instability arising from the convergence of meridians at the polar points on latitude-longitude grids (e.g., Figure 1a). Depending on the numerics, methods exist to stabilize the pole problem, and latitude-longitude grids may be advantageous for polar processes as structures can be represented with more degrees of freedom than elsewhere in the computational domain. With the recent trend towards globally uniform unstructured grids, any potential benefits of latitude-longitude grids on polar regions may become a relic of the past. In this study, a spectrum of grids and dynamical cores (hereafter referred to as *dycores*) available in the Community Earth System Model, version 2.2 (CESM; <http://www.cesm.ucar.edu/models/cesm2/>), from conventional latitude-longitude grids to unstructured grids with globally uniform grid spacing to unstructured grids with regional refinement over the Arctic, are evaluated to understand their impacts on the simulated characteristics of the Arctic, with a special focus on the Greenland Ice Sheet.

In the 1970's the pole problem was largely defeated through wide-spread adoption of efficient spectral transform methods in GCMs. These methods transform grid point fields into a global, isotropic representation in wave space, where linear operators in the equation set can be solved for exactly. While spectral transform methods are still commonly used in the 21st century, local numerical methods have become desirable for their ability to run efficiently on massively parallel systems. The pole-problem has thus re-emerged in contemporary climate models that use latitude-longitude grids, and some combination of reduced grids and polar filters are necessary to ameliorate this instability (Jablonowski & Williamson, 2011). Polar filters are akin to a band-aid; they subdue the growth of unstable modes by applying additional damping to the solution over polar regions. One might expect that this additional damping reduces the effective resolution such that the resolved scales are similar across the entire domain, but this seems an unlikely and is explored further in this study.

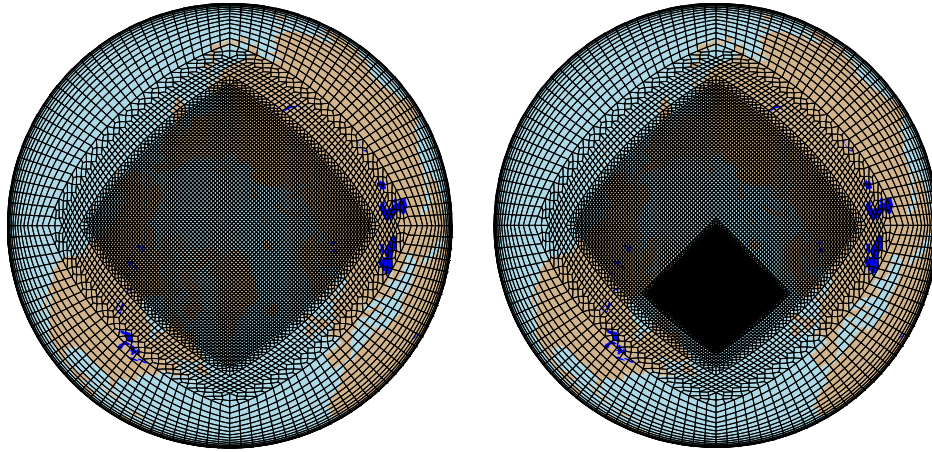
An alternative approach is to use unstructured grids. Unstructured grids allow for more flexible grid structures, permitting quasi-uniform grid spacing globally that eliminates the pole-problem entirely (e.g., Figure 1c). This grid flexibility also allows for variable-resolution or regional grid refinement. Grids can be developed with refinement over polar regions that could in principle make up for any loss in polar resolution in transitioning away from latitude-longitude grids (e.g., Figure 2), although this comes at the cost of a smaller CFL-limiting time-step in the refined region. But unstructured grids scale more efficiently on parallel systems than latitude-longitude grids, resulting in latitude-longitude grids becoming less common, and unstructured grids more common as computing power continued to increase over time.

The meteorology and climate of the Arctic is characterized by a range of processes and scales that are difficult to represent in GCMs (Bromwich et al., 2001; Smirnova & Golubkin, 2017; van Kampenhout et al., 2018). Synoptic scale storms are well represented

**Figure 1.** .

at typical GCM resolutions, but mesoscale Polar Lows are not. These mesoscale systems are prevalent during the cold season, and produce gale-force winds that can induce large fluxes through the underlying sea-ice/ocean interface. The Arctic also contains the Greenland Ice Sheet (hereafter denoted as *GrIS*). While it blankets the largest island in the world (Greenland), *GrIS* is only marginally resolved at typical GCM resolutions. *GrIS* ablation zones exert a primary control on the mass balance of the ice sheet, but are on the order of 100km wide, and models struggle to resolve these narrow features. *GrIS* elevations descend rapidly toward the coasts, resulting in steep margins that facilitate orographic precipitation events, but which are not well resolved in GCMs. The Arctic is therefore well-suited to understand the impact of different grids and dycores on processes that are marginally resolved at conventional GCM resolutions.

The goal of this study is to characterize the representation of high-latitude regions using the spectral-element and finite-volume dycores in CESM2.2, as these models treat the high-latitudes, e.g., the pole-problem, in very different ways. The manuscript is laid out as follows. Section 2 consists of documentation of the grids, dycores and physical parameterizations used in this study. The Arctic refined grids were developed by the authors, and this section serves as their official documentation in CESM2.2. Section 2 also contains a description of the experiments along with the observational datasets and post-processing software used for evaluating the models. Section 3 contains the results of the experiments and Section 4 provides some discussion and conclusions.

**Figure 2.**

## 2 Methods

### 2.1 Dynamical cores

The atmospheric component of CESM2.2, the Community Atmosphere Model, version 6.3 (CAM; <https://ncar.github.io/CAM/doc/build/html/index.html>), supports a diverse number of atmospheric dynamical cores. These range from dycores using latitude-longitude grids, the finite-volume (FV; Lin, 2004) and eulerian spectral transform (EUL; Collins et al., 2006) models, and dycores built on unstructured grids, the spectral-element (SE; Lauritzen et al., 2018) and finite-volume 3 (FV3; Putman & Lin, 2007) models. The EUL dycore is the oldest dycore in CAM, and the least supported of all the dycores in the current model. FV3 is the newest dycore in CAM, but it was not fully incorporated at the time this work commenced, and so is omitted from this study. The authors instead focus on the two most well supported dycores in CAM, SE and FV.

#### 2.1.1 Finite-volume dynamical core

The FV dycore is a hydrostatic model that integrates the equations of motion using a finite-volume discretization on a spherical latitude-longitude grid (Lin & Rood, 1997). The 2D dynamics evolve in floating Lagrangian layers that are periodically mapped to Eulerian reference grid in the vertical (Lin, 2004), using a hybrid-pressure vertical coordinate. Hyperviscous damping is applied to the divergent modes while Laplacian damping is applied to momentum in the top few layers, referred to as a *sponge layer* (Lauritzen et al., 2011). A polar filter is used to avoid computational instability due to the convergence of the meridians, allowing for a more practical time-step. It takes the form of a Fourier filter in the zonal direction, with the damping coefficients increasing monotonically poleward (Suarez & Takacs, 1995).

#### 2.1.2 Spectral-element dynamical core

The SE dycore is a hydrostatic model that integrates the equations of motion using a high-order continuous Galerkin method (Taylor et al., 1997; Dennis et al., 2012). The computational domain is a cubed-sphere grid tiled with quadrilateral elements (e.g., Figure 2). Each element contains a fourth order basis set in the two horizontal directions, with the solution defined at the roots of the basis functions, the Gauss-Lobatto-Legendre (GLL) quadrature points. This results in 16 GLL nodal points within each element, with

109 12 of the points lying on the (shared) element boundary. Communication between el-  
 110 ements happens via the direct stiffness summation (Canuto et al., 2007), which applies  
 111 a numerical flux to the element boundaries that reconciles overlapping nodal point val-  
 112 ues and produces a continuous global basis set.

113 As with the FV dycore, the dynamics evolve in floating Lagrangian layers that are  
 114 subsequently mapped to a Eulerian reference grid. A dry mass vertical coordinate was  
 115 more recently implemented for thermodynamic consistency with condensates (Lauritzen  
 116 et al., 2018). The 2D dynamics have no implicit dissipation and so hyperviscosity op-  
 117 erators are applied to all prognostic variables to remove spurious numerical errors (Dennis  
 118 et al., 2012). Laplacian damping is applied in the sponge layer.

119 The SE dycore supports regional grid refinement via its variable-resolution config-  
 120 uration, requiring two enhancements over uniform resolution grids. (1) As the numer-  
 121 ical viscosity increases with resolution, explicit hyperviscosity relaxes according to the  
 122 local element size, reducing in strength by about an order of magnitude per halving of  
 123 the grid spacing. A tensor-hyperviscosity formulation is used (Guba et al., 2014), which  
 124 adjusts the coefficients in two orthogonal directions to more accurately target highly dis-  
 125 torted quadrilateral elements. (2) The topography boundary conditions need to be smoothed  
 126 in a way that does not excite grid scale modes, and so the NCAR topography software  
 127 (Lauritzen et al., 2015) was modified to scale the smoothing radius by the local element  
 128 size.

129 For spectral-element grids with quasi-uniform grid spacing, a variant in which tracer  
 130 advection is computed using the Conservative Semi-Lagrangian Mult-tracer tranport  
 131 scheme is used instead (CSLAM; Lauritzen et al., 2017). CSLAM has improved tracer  
 132 property preservation and accelerated multi-tracer transport. It uses a seperate grid from  
 133 the spectral-element dynamics, through dividing each element into  $3 \times 3$  quasi-equal area  
 134 control volumes. The physical parameterizations are computed from the state on the CSLAM  
 135 grid, which has clear advantages over the default SE dycore in which the physics are eval-  
 136 uated at the GLL nodal points (A. Herrington et al., 2018).

## 137 2.2 Grids

138 Six grid are evaluated in this study (Table X). The FV dycore is run with  $1^\circ$  and  
 139  $2^\circ$  grid spacing, referred to as  $f09$  and  $f19$ , respectively (Figure 1a,b). The  $1^\circ$  equiv-  
 140 alent of the CAM-SE-CSLAM grid is also run, referred to as  $ne30pg3$  (Figure 1c), where  
 141  $ne$  refers to a grid with of  $ne \times ne$  elements per cubed-sphere face, and  $pg$  denotes that  
 142 there are  $pg \times pg$  control volumes per element for computing the physics. An additional  
 143  $1^\circ$  CAM-SE-CSLAM grid is run, but with the physical paramerizations computed on a  
 144 grid that contains  $2 \times 2$  control volumes per element,  $ne30pg2$  (Figure 1d; A. R. Her-  
 145 rington et al., 2019).

146 Two variable resolution meshes were developed as part of the CESM2.2 release that  
 147 contains grid refinement over the Arctic (Figure 2). The Arctic meshes were developed  
 148 using the software package SQuadgen (<https://github.com/ClimateGlobalChange/squadgen>). The *ARCTIC* grid is a  $1^\circ$  grid with  $\frac{1}{4}^\circ$  regional refinement over the broader  
 149 Arctic region. The *ARCTICGRIS* grid is identical to the *ARCTIC* grid, but contains  
 150 an additional patch covering the big island of Greenland with  $\frac{1}{8}^\circ$  resolution.

## 152 2.3 Physical parameterizations

153 The CAM6 physical parameterization package (hereafter referred to as the *physics*;  
 154 <https://ncar.github.io/CAM/doc/build/html/index.html>) is used for all simula-  
 155 tions in this study. CAM6 physics is most noteably different from it's predecessors through  
 156 the incorporation of high-order turbulence closure, Cloud Layers Unified by Binormals  
 157 (CLUBB; Golaz et al., 2002; Bogenschutz et al., 2013), which jointly acts as a PBL, shal-

158 low convection and cloud macrophysics scheme. CLUBB is coupled with the MG2 microphysics scheme (Gettelman et al., 2015), with prognostic precipitation and classical  
 159 nucleation theory in representing cloud ice for improved cloud-aerosol interactions. Deep  
 160 convection is parameterized using a convective quasi-equilibrium mass flux scheme (Zhang  
 161 & McFarlane, 1995; Neale et al., 2008) including convective momentum transport (Richter  
 162 et al., 2010). PBL form drag is modeled after (Beljaars et al., 2004) and orographic gravity  
 163 wave drag is represented with an anisotropic method informed by the orientation of  
 164 topographic ridges at the sub-grid scale.  
 165

## 166 2.4 Experimental design

167 All grids and dycores are run using an identical transient 1979-1998 AMIP-style  
 168 configuration, with prescribed monthly SST/sea-ice after (Hurrell et al., 2008). This configura-  
 169 tion refers to the *FHIST compset* and runs out of the box in CESM2.2. The Com-  
 170 munity Land Model (CLM5; [https://escomp.github.io/ctsm-docs/versions/release](https://escomp.github.io/ctsm-docs/versions/release-clm5.0/html/users_guide/index.html)  
 171 -clm5.0/html/users\_guide/index.html), which uses the same grid as the atmosphere  
 172 grid, calculates the surface energy balance at each land tile within a grid cell, which is  
 173 used to compute snow and bare ice melting to inform the surface mass balance (SMB)  
 174 of a glacier unit (van Kampenhout et al., 2020). Ice accumulation is modeled as a cap-  
 175 ping flux, or snow in excess of the assumed 10 m snow cap, and refreezing of liquid within  
 176 the snowpack additionally acts as a source of mass in the SMB calculation. Since the  
 177 10 m snowcap needs to be reached in the accumulation zone to simulate the SMB, the  
 178 snow depths in the variable-resolution grids were spun-up by forcing CLM5 offline, cy-  
 179 cling over 20 years of a fully coupled *ARCTIC* run for about 500 years. The uniform  
 180 resolution grids are all initialized with an SMB from an existing *f09* spun-up initial con-  
 181 dition.

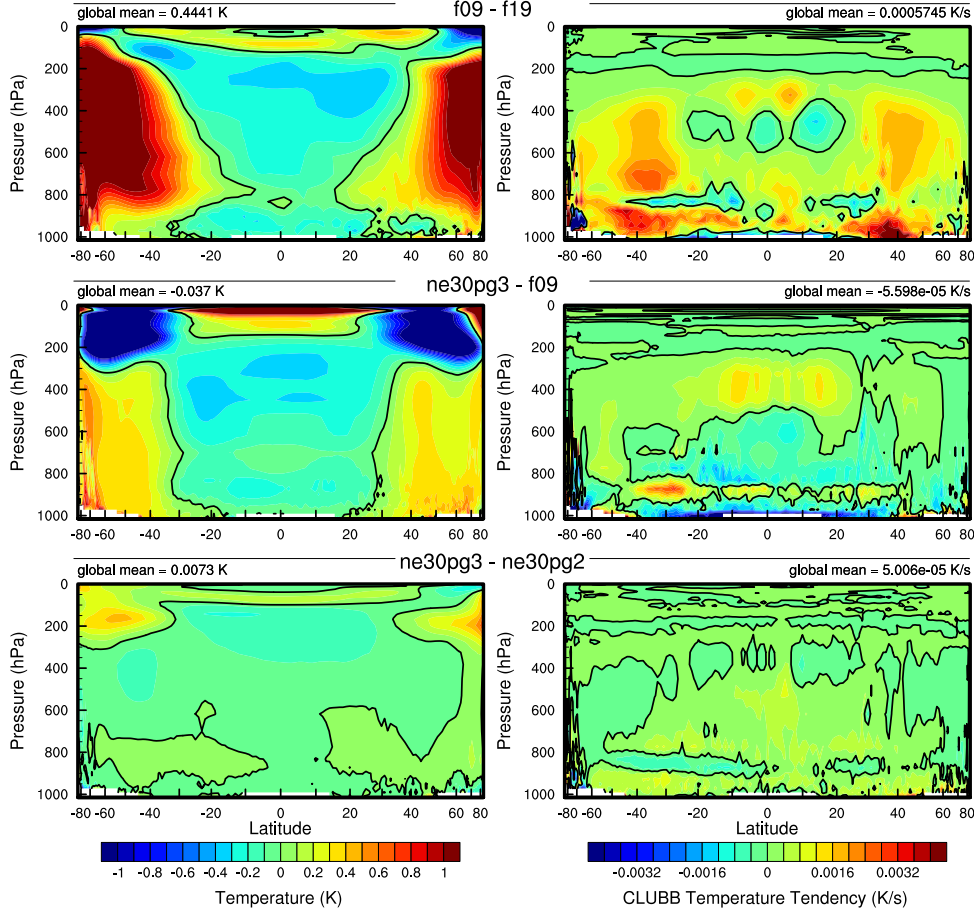
## 182 3 Results

### 183 3.1 Tropospheric temperatures

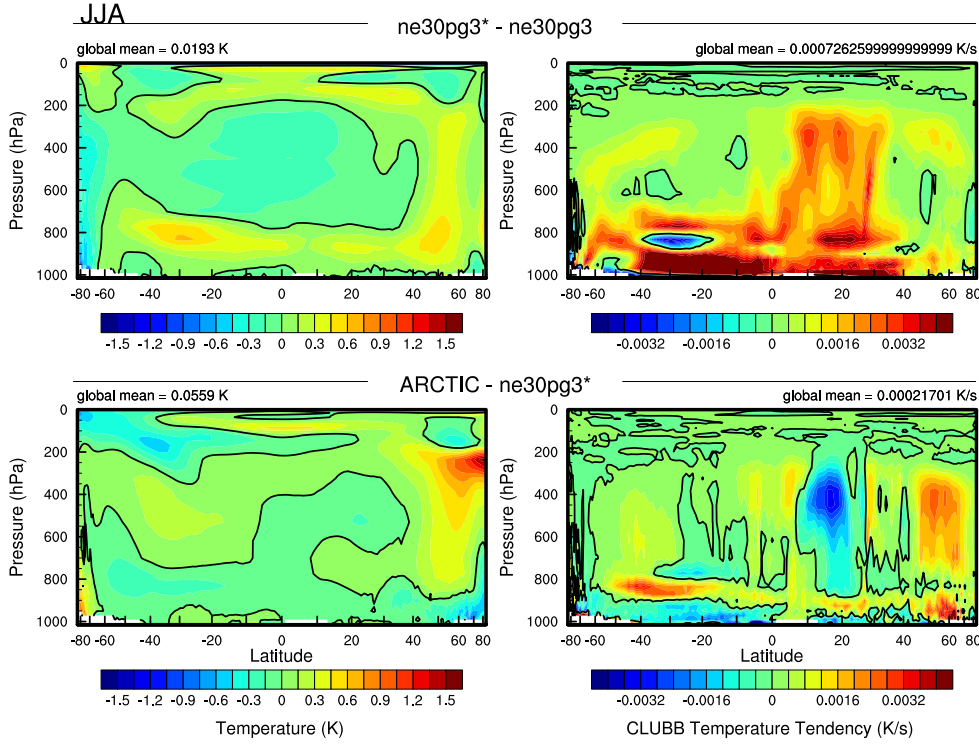
184 Before delving into the simulated characteristics of the Arctic, an understanding  
 185 of the global mean differences between the grids and dycores are assessed, Figure 3 shows  
 186 the climatological, zonal mean height plots expressed as differences between the uniform  
 187 resolution grids and dycores. The *f09* grid is warmer than the *f19* grid, primarily in the  
 188 mid-to-high latitudes and throughout the depth of the troposphere. This is common re-  
 189 sponse to increasing horizontal resolution in GCMs (Pope & Stratton, 2002; Roeckner  
 190 et al., 2006), and (A. R. Herrington & Reed, 2020) has shown that this occurs in CAM  
 191 due to greater resolved vertical velocities that in turn, facilitate greater condensational  
 192 heating in the macrophyics routine in CLUBB. The right columns in Figure 3 supports  
 193 this interpretation, which shows an increase in the climatological CLUBB heating in the  
 194 mid-latitudes in the *f09* grid.

195 As the SE dycore is less diffusive than the FV dycore, the resolved vertical veloc-  
 196 ities are larger in the SE dycore, and so a modest, resolution-like sensitivity occurs in  
 197 which *ne30pg3* is warmer than *f09* (Figure 3). The stratosphere has a different signal,  
 198 in which *ne30pg3* is much cooler than *f09* in the mid-to-high latitudes. The differences  
 199 in temperature between *ne30pg3* and *ne30pg2* are small, with a slight warming near the  
 200 tropopause at high latitudes. This is consistent with the similar climates using these grids  
 201 shown in (A. R. Herrington et al., 2019).

202 In comparing the variable-resolution grids to the uniform resolution grids is con-  
 203 voluted because not only is the resolution higher in refinement region, but the physics  
 204 time-step is shorter in the variable-resolution runs. An additional *ne30pg3* simulations  
 205 was run with physics time-step used in the *ARCTIC* grid, referred to as *ne30pg3\**. Fig-  
 206 ure 4 shows the changes in climatological temperature in zonal-mean height space be-

**Figure 3.**

207      between *ne30pg3\** and *ne30pg3*. A similar warming response to increase resolution occurs  
 208      when the time-step is reduced, and the mechanism is similar in that this facilitates greater  
 209      condensational heating by CLUBB. Figure 4 shows difference in climatological temper-  
 210      ature between the *ARCTIC* grid and the *ne30pg3\** grid. The greater condensational heat-  
 211      ing and warmer temperatures are confined to the regionally refined region when the im-  
 212      pact of physics time-steps is removed from the analysis.

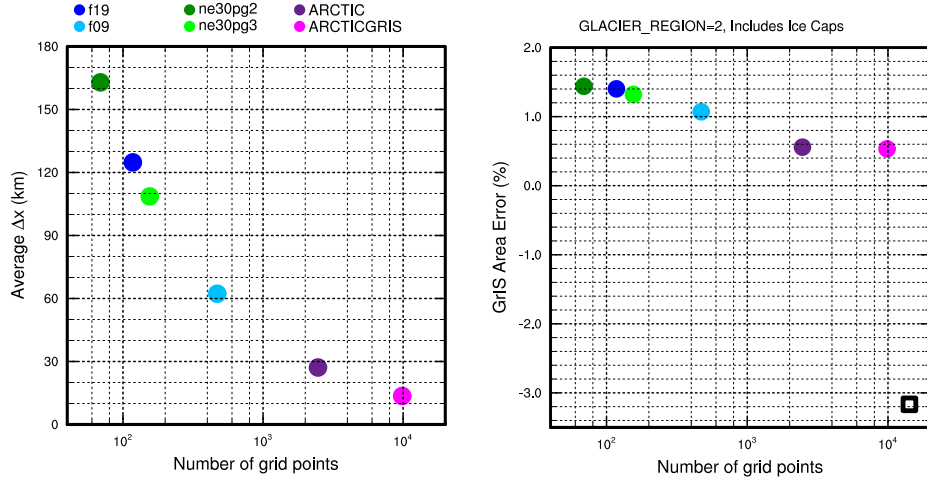
**Figure 4.**213 **3.2 Inter-annual variability**214 **3.3 Synoptic-scale storm characteristics**215 **3.4 Orographic gravity waves emanating from Greenland**216 **3.5 Katabatic winds emanating from Greenland**217 **3.6 Greenland surface mass balance**218 **4 Conclusions**219 **Acknowledgments**

220 This material is based upon work supported by the National Center for Atmospheric Re-  
 221 search (NCAR), which is a major facility sponsored by the NSF under Cooperative Agree-  
 222 ment 1852977. Computing and data storage resources, including the Cheyenne super-  
 223 computer (doi:10.5065/D6RX99HX), were provided by the Computational and Infor-  
 224 mation Systems Laboratory (CISL) at NCAR.

225 The data presented in this manuscript is available at <https://github.com/adamrher/>  
 226 2020-arcticgrids.

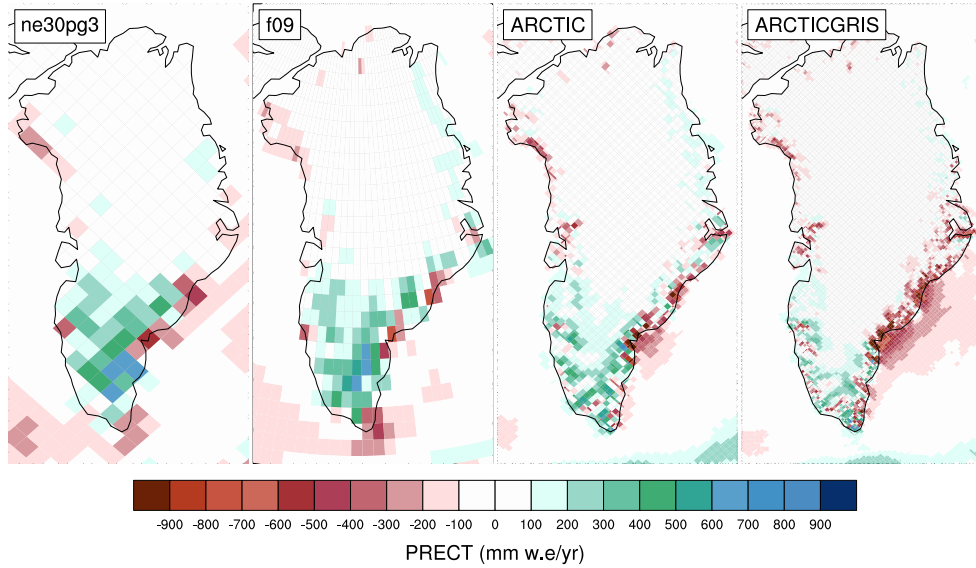
227 **References**

- 228 Beljaars, A., Brown, A., & Wood, N. (2004). A new parametrization of turbulent  
 229 orographic form drag. *Quart. J. Roy. Meteor. Soc.*, *130*(599), 1327–1347. doi:  
 230 10.1256/qj.03.73



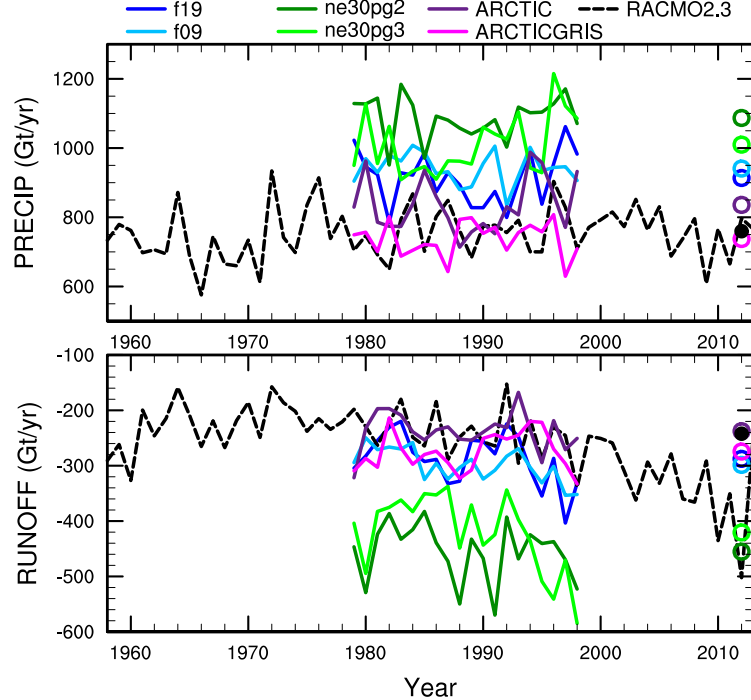
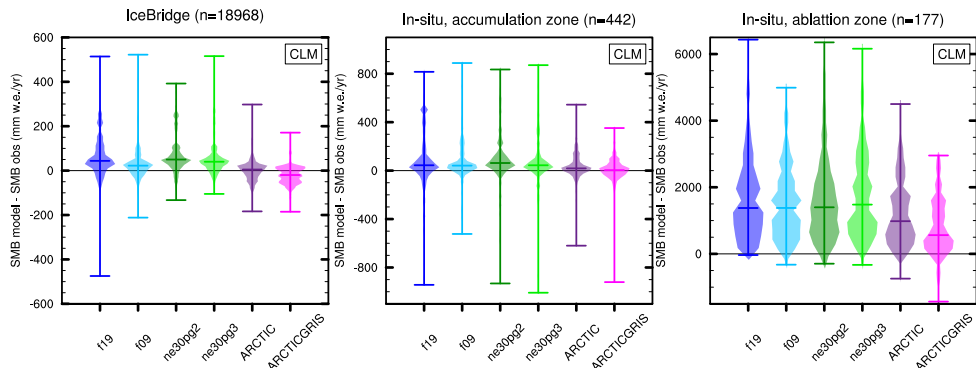
**Figure 5.** .

ANN Climo (1979-1998) minus RACMO ANN Climo (1979-1998)

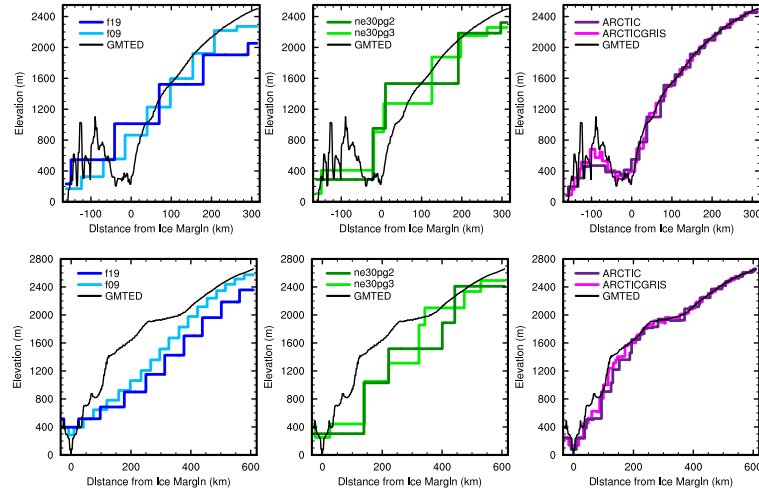
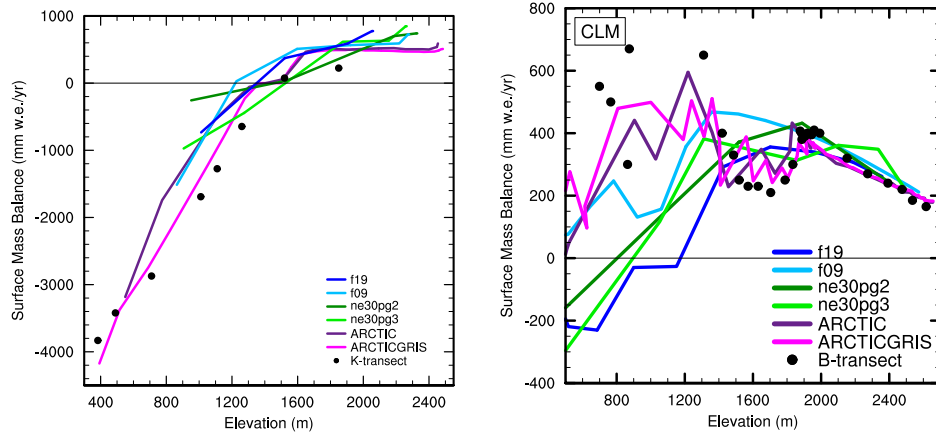


**Figure 6.** .

- 231 Bogenschutz, P. A., Gettelman, A., Morrison, H., Larson, V. E., Craig, C., & Scha-  
 232 nnen, D. P. (2013). Higher-order turbulence closure and its impact on climate  
 233 simulations in the community atmosphere model. *Journal of Climate*, 26(23),  
 234 9655–9676.  
 235 Bromwich, D. H., Cassano, J. J., Klein, T., Heinemann, G., Hines, K. M., Steffen,  
 236 K., & Box, J. E. (2001). Mesoscale modeling of katabatic winds over greenland  
 237 with the polar mm5. *Monthly Weather Review*, 129(9), 2290–2309.  
 238 Canuto, C., Hussaini, M. Y., Quarteroni, A., & Zang, T. (2007). *Spectral methods:*  
 239 *Evolution to complex geometries and applications to fluid dynamics* (1st ed.).  
 Springer.  
 240 Collins, W. D., Rasch, P. J., Boville, B. A., Hack, J. J., McCaa, J. R., Williamson,  
 241 D. L., ... Zhang, M. (2006). The formulation and atmospheric simulation

**Figure 7.****Figure 8.**

- of the community atmosphere model version 3 (cam3). *Journal of Climate*, 19(11), 2144–2161.
- Dennis, J. M., Edwards, J., Evans, K. J., Guba, O., Lauritzen, P. H., Mirin, A. A., ... Worley, P. H. (2012). CAM-SE: A scalable spectral element dynamical core for the Community Atmosphere Model. *Int. J. High. Perform. C.*, 26(1), 74–89. Retrieved from <http://hpc.sagepub.com/content/26/1/74.abstract> doi: 10.1177/1094342011428142
- Gettelman, A., Morrison, H., Santos, S., Bogenschutz, P., & Caldwell, P. (2015). Advanced two-moment bulk microphysics for global models. part ii: Global model solutions and aerosol–cloud interactions. *Journal of Climate*, 28(3), 1288–1307.
- Golaz, J.-C., Larson, V. E., & Cotton, W. R. (2002). A pdf-based model for bound-

**Figure 9.** .**Figure 10.** .

- 255         ary layer clouds. part i: Method and model description. *Journal of the Atmospheric Sciences*, 59(24), 3540–3551. doi: 10.1175/1520-0469(2002)059<3540:apbmfb>2.0.co;2
- 256         Guba, O., Taylor, M. A., Ullrich, P. A., Overfelt, J. R., & Levy, M. N. (2014). The  
257         spectral element method (sem) on variable-resolution grids: evaluating grid  
258         sensitivity and resolution-aware numerical viscosity. *Geosci. Model Dev.*, 7(6),  
259         2803–2816. doi: 10.5194/gmd-7-2803-2014
- 260         Herrington, A., Lauritzen, P., Taylor, M. A., Goldhaber, S., Eaton, B. E., Bacmeis-  
261         ter, J., ... Ullrich, P. (2018). Physics-dynamics coupling with element-based  
262         high-order galerkin methods: quasi equal-area physics grid. *Mon. Wea. Rev.*,  
263         47, 69–84. doi: 10.1175/MWR-D-18-0136.1
- 264         Herrington, A. R., Lauritzen, P. H., Reed, K. A., Goldhaber, S., & Eaton, B. E.  
265         (2019). Exploring a lower resolution physics grid in cam-se-cslam. *Journal of  
266         Advances in Modeling Earth Systems*, 11.
- 267         Herrington, A. R., & Reed, K. A. (2020). On resolution sensitivity in the commu-  
268         nity atmosphere model. *Quarterly Journal of the Royal Meteorological Society*,  
269         146(733), 3789–3807.

- 272 Hurrell, J. W., Hack, J. J., Shea, D., Caron, J. M., & Rosinski, J. (2008). A new  
 273 sea surface temperature and sea ice boundary dataset for the community at-  
 274 mosphere model. *Journal of Climate*, 21(19), 5145–5153.
- 275 Jablonowski, C., & Williamson, D. L. (2011). The pros and cons of diffusion, fil-  
 276 ters and fixers in atmospheric general circulation models., in: P.H. Lauritzen,  
 277 R.D. Nair, C. Jablonowski, M. Taylor (Eds.), Numerical techniques for global  
 278 atmospheric models. *Lecture Notes in Computational Science and Engineering*,  
 279 Springer, 80.
- 280 Lauritzen, P. H., Bacmeister, J. T., Callaghan, P. F., & Taylor, M. A. (2015). Ncar  
 281 global model topography generation software for unstructured grids. *Geosci-  
 282 entific Model Development Discussions*, 8(6), 4623–4651. doi: 10.5194/gmdd-8  
 283 -4623-2015
- 284 Lauritzen, P. H., Mirin, A., Truesdale, J., Raeder, K., Anderson, J., Bacmeister, J.,  
 285 & Neale, R. B. (2011). Implementation of new diffusion/filtering operators  
 286 in the CAM-FV dynamical core. *Int. J. High Perform. Comput. Appl.*. doi:  
 287 10.1177/1094342011410088
- 288 Lauritzen, P. H., Nair, R., Herrington, A., Callaghan, P., Goldhaber, S., Dennis, J.,  
 289 ... Dubos, T. (2018). NCAR CESM2.0 release of CAM-SE: A reformulation  
 290 of the spectral-element dynamical core in dry-mass vertical coordinates with  
 291 comprehensive treatment of condensates and energy. *J. Adv. Model. Earth  
 292 Syst.*. doi: 10.1029/2017MS001257
- 293 Lauritzen, P. H., Taylor, M. A., Overfelt, J., Ullrich, P. A., Nair, R. D., Goldhaber,  
 294 S., & Kelly, R. (2017). CAM-SE-CSLAM: Consistent coupling of a conser-  
 295 vative semi-lagrangian finite-volume method with spectral element dynamics.  
 296 *Mon. Wea. Rev.*, 145(3), 833-855. doi: 10.1175/MWR-D-16-0258.1
- 297 Lin, S.-J. (2004). A 'vertically Lagrangian' finite-volume dynamical core for global  
 298 models. *Mon. Wea. Rev.*, 132, 2293-2307.
- 299 Lin, S.-J., & Rood, R. B. (1997). An explicit flux-form semi-Lagrangian shallow-  
 300 water model on the sphere. *Q.J.R.Meteorol.Soc.*, 123, 2477-2498.
- 301 Neale, R. B., Richter, J. H., & Jochum, M. (2008). The impact of convection on  
 302 ENSO: From a delayed oscillator to a series of events. *J. Climate*, 21, 5904-  
 303 5924.
- 304 Pope, V., & Stratton, R. (2002). The processes governing horizontal resolution sensi-  
 305 tivity in a climate model. *Climate Dynamics*, 19(3-4), 211–236.
- 306 Putman, W. M., & Lin, S.-J. (2007). Finite-volume transport on various cubed-  
 307 sphere grids. *J. Comput. Phys.*, 227(1), 55-78.
- 308 Richter, J. H., Sassi, F., & Garcia, R. R. (2010). Toward a physically based gravity  
 309 wave source parameterization in a general circulation model. *J. Atmos. Sci.*,  
 310 67, 136-156. doi: dx.doi.org/10.1175/2009JAS3112.1
- 311 Roeckner, E., Brokopf, R., Esch, M., Giorgetta, M., Hagemann, S., Kornblueh, L.,  
 312 ... Schulzweida, U. (2006). Sensitivity of simulated climate to horizontal  
 313 and vertical resolution in the echam5 atmosphere model. *Journal of Climate*,  
 314 19(16), 3771–3791.
- 315 Smirnova, J., & Golubkin, P. (2017). Comparing polar lows in atmospheric reanal-  
 316 yses: Arctic system reanalysis versus era-interim. *Monthly Weather Review*,  
 317 145(6), 2375–2383.
- 318 Suarez, M. J., & Takacs, L. L. (1995). Volume 5 documentation of the aries/geos dy-  
 319 namical core: Version 2.
- 320 Taylor, M. A., Tribbia, J., & Iskandarani, M. (1997). The spectral element method  
 321 for the shallow water equations on the sphere. *J. Comput. Phys.*, 130, 92-108.
- 322 van Kampenhout, L., Lenaerts, J. T., Lipscomb, W. H., Lhermitte, S., Noël, B.,  
 323 Vizcaíno, M., ... van den Broeke, M. R. (2020). Present-day greenland ice  
 324 sheet climate and surface mass balance in cesm2. *Journal of Geophysical  
 325 Research: Earth Surface*, 125(2), e2019JF005318.
- 326 van Kampenhout, L., Rhoades, A. M., Herrington, A. R., Zarzycki, C. M., Lenaerts,

- 327 J. T. M., Sacks, W. J., & van den Broeke, M. R. (2018). Regional grid refine-  
328 ment in an earth system model: Impacts on the simulated greenland surface  
329 mass balance. *The Cryosphere Discuss.*. doi: 10.5194/tc-2018-257
- 330 Williamson, D. (2007). The evolution of dynamical cores for global atmospheric  
331 models. *J. Meteor. Soc. Japan*, 85, 241-269.
- 332 Zhang, G., & McFarlane, N. (1995). Sensitivity of climate simulations to the pa-  
333 rameterization of cumulus convection in the canadian climate centre general  
334 circulation model. *Atmosphere-ocean*, 33(3), 407-446.